PRE-PRINT of the article "Briggen P, Blocken B, Schellen HL. 2009. Wind-driven rain on the facade of a monumental tower: numerical simulation, full-scale validation and sensitivity analysis. **Building and Environment** 44(8): 1675–1690.

Wind-driven rain on the facade of a monumental tower: numerical simulation, full-scale validation and sensitivity analysis

P.M. Briggen, B. Blocken*, H.L. Schellen

Building Physics and Systems, Eindhoven University of Technology, P.O. box 513, 5600 MB Eindhoven, the Netherlands

Abstract

Wind-driven rain (WDR) is one of the most important moisture sources that affect the hygrothermal performance and the durability of building facades. The facades of the Dutch monumental building St. Hubertus show severe deterioration caused by WDR. Assessment of the amount and intensity of WDR falling onto the facades is necessary as input for numerical heat-air-moisture (HAM) transfer models to analyse the causes of the moisture problems and the impact of remedial measures. In this study, a numerical simulation method based on Computational Fluid Dynamics (CFD) is used to predict the amount of WDR impinging on the south-west facade of the tower of the building. The paper focuses on the numerical simulation results, the validation of these results and their sensitivity to two parameters: the level of geometrical detailing of the computational building model and the upstream terrain aerodynamic roughness length. Validation is performed by comparison of the numerical results with a dataset obtained from on-site WDR measurements. It is shown that the CFD simulations provide fairly good predictions of the amount of WDR impinging on the south-west facade of the tower, except for the lower part. It is also shown that the local effects of geometrical facade details are significant and can yield differences in WDR exposure up to 40%, while their effect at other positions is negligible. Finally, the sensitivity of WDR simulations to the upstream aerodynamic roughness length is discussed.

Keywords: Driving rain; Experimental data; Field measurements; Raindrop trajectory; Numerical simulation; Hygrothermal modelling.

1. Introduction

Building Physics aims at providing a healthy, comfortable and sustainable indoor and outdoor environment of buildings. Sustainability also involves the durability of the building envelope that separates the indoor and the outdoor environment. Wind-driven rain (WDR) is one of the most important moisture sources that affect the hygrothermal performance and the durability of building facades [1-5]. Numerical analysis of the hygrothermal behaviour with so-called HAM (heat-air-moisture) models requires accurate WDR data as boundary condition [1-8].

Three categories of methods exist for determining the WDR intensity that impinges on building facades: (1) measurements, (2) semi-empirical methods and (3) numerical methods based on Computational Fluid Dynamics (CFD). A literature review of each of these categories has been provided by Blocken and Carmeliet [5]. Measurements have always been the primary tool in WDR research, but are nowadays only rarely conducted. The most important reason is the fact that WDR measurements can easily suffer from large errors [3,9-11]. Recently, guidelines have been proposed that should be followed for selecting accurate and reliable WDR data from experimental WDR datasets [10,11]. The strict character of these guidelines, however, implies that only very few rain events in a WDR dataset are accurate and reliable and hence suitable for WDR studies. Other drawbacks of WDR measurements are the fact that they are time-consuming and the fact that measurements conducted at a particular building site have very limited application to other sites. Semi-empirical methods are an alternative to measurements. The main advantage of semi-empirical methods is their ease-of-use; their main disadvantage is that generally only rough estimates of the WDR exposure can be obtained [5]. Given the limitations of measurements and semi-empirical methods, in the past decades, numerical simulation with CFD has been explored. Choi [12-14] developed and applied a steady-state numerical simulation technique based on CFD. It allows determining the spatial distribution of WDR on building facades for given (fixed) values of the wind speed, the wind direction and the horizontal rainfall intensity. Later, Choi's simulation technique was extended into the time domain by Blocken and Carmeliet [15,16]. In all of these studies, CFD simulations were based on the Reynolds-Averaged Navier-Stokes (RANS) equations.

* Corresponding author: Bert Blocken, Building Physics and Systems, Eindhoven University of Technology, P.O. box 513, 5600 MB Eindhoven, The Netherlands. Tel. +31 (0)40 247 2138 - Fax +31 (0)40 243 8595. *E-mail address:* b.j.e.blocken@tue.nl

Validation is an essential part of RANS CFD simulations. Up to now, only a few attempts have been made for CFD validation with full-scale WDR measurements [3,5,15,17-19]. Van Mook [3] was the first to compare simulations with full-scale measurements at a few selected positions at the west facade of a wide, high-rise building. Blocken and Carmeliet [15,18] performed CFD WDR validation for a low-rise building with a sloped and a flat roof module, based on measurements with 24 WDR gauges installed at the south-west and north-west facades. Tang and Davidson [17] validated numerical simulations for the rather complex Cathedral of Learning with WDR measurements at 16 different positions. Most recently, Abuku et al. [19] employed the WDR measurement data by Nore et al. [20] for the validation of WDR simulations on the west facade of a low-rise rectangular test building with various angles of wind incidence. While some authors found significant discrepancies between simulations and measurements [3], others indicated a fair to good agreement [15,17-19].

While these efforts have provided valuable information, the need for additional WDR measurement data and CFD validation studies is still present, in particular for different types of buildings in different environment topographies [11,18]. This need is driven by the complex nature of WDR and the wide range of influencing parameters. Additionally, sensitivity studies are needed concerning the large amount of computational parameters that have to be set by the user in such CFD simulations. Two important questions are: (1) to what extent do geometrical facade details have to be included in the computational model of the building; and (2) how sensitive are the results to the estimate of the aerodynamic roughness length of the upstream terrain. The inclusion of facade details can present a challenge in CFD WDR studies, due to the large difference in length scales between the computational domain (up to several 100 m or km) and the facade details (down to a few cm) and the subsequent need for very fine grids near the building surface. The aerodynamic roughness length determines the shape of the inlet profiles of mean wind speed, turbulent kinetic energy and turbulence dissipation rate, as well as the physical roughness height k_S that has to be applied at the bottom of the computational domain [21]. It is generally estimated from the updated Davenport roughness classification by Wieringa [22], based on a fetch (upstream distance) of at least 5 km (Table 1). However, estimating a representative aerodynamic roughness length for heterogeneous terrain is difficult, and it is therefore rather easy to be one class off in this roughness classification.

In this paper, CFD simulations of WDR on the south-west facade of the tower of Hunting Lodge St. Hubertus (Fig. 1a) are performed. It is a monumental building situated in the National Park “De Hoge Veluwe”. Especially the south-west facade of the building shows severe deterioration caused by WDR and subsequent phenomena such as rain penetration, mould growth, frost damage, salt crystallization and efflorescence, and cracking due to hygrothermal gradients (Fig. 1b-e). The CFD WDR simulations are important to obtain accurate spatial and temporal distribution records of WDR, to be used as input for numerical HAM transfer simulations. These simulations will be used in a later stage to analyse the causes of the moisture problems and to assess the impact of remedial measures. Validation of the CFD simulations is performed by WDR measurements at a few selected locations at the south-west facade. In addition, the influence of neglecting all protruding and recessed facade details and of shifting the estimated upstream aerodynamic roughness length one class higher or lower, is investigated. This can provide some guidance for future CFD WDR simulations.

In section 2 of the paper, the definitions of the specific catch ratio, the catch ratio and the influencing parameters are given. The building geometry and the surrounding topography are described in section 3. In section 4, the measurement set-up for wind, rain and WDR is described. The extended WDR simulation model, the simulation characteristics and settings and the selected rain events are described in section 5. The simulation results are compared with the measurements in section 6. This section also contains the results of the sensitivity study. The paper ends with a discussion (section 7) and the conclusions (section 8).

2. Wind-driven rain: definitions and parameters

The quantities that are used to describe the WDR intensity in numerical simulations are the specific catch ratio $\eta_d(d)$, related to the raindrop diameter d, and the catch ratio η, related to the entire spectrum of raindrop diameters:

$$\eta_d(d) = \frac{R_{wdr}(d)}{R_h(d)}; \qquad \eta = \frac{R_{wdr}}{R_h} \tag{1}$$

where $R_{wdr}(d)$ and $R_h(d)$ are the specific WDR intensity on the building and the specific unobstructed horizontal rainfall intensity (for raindrop diameter d), respectively. R_{wdr} and R_h are the WDR intensity on the building and the unobstructed horizontal rainfall intensity, integrated over all raindrop diameters. The unobstructed horizontal rainfall intensity is the intensity of rainfall through a horizontal plane situated outside the wind-flow pattern that is disturbed by the presence of the building. All rain intensities are given in mm/h.

The catch ratio η is a complicated function of time and space. The six basic influencing parameters for η are: (1) the building geometry (including environment topography), (2) the position on the building facade, (3) the

reference wind speed, (4) the reference wind direction, (5) the horizontal rainfall intensity and (6) the horizontal raindrop-size distribution. The turbulent dispersion of raindrops is an additional parameter, which is often neglected. Turbulent dispersion means that raindrop trajectories will deviate from those that would be calculated based on the mean wind-velocity field only. The turbulent dispersion of raindrops is neglected in this study, based on the findings by Choi [23], by Blocken and Carmeliet [15] and on a review of the literature [5]. The reference wind speed U (m/s) is taken as the horizontal component of the wind-velocity vector at 10 m height in the upstream undisturbed flow (U_{10}). The reference wind direction φ_{10} (degrees from north) refers to the direction of the reference wind speed at 10 m height. The horizontal raindrop-size distribution $f_h(d)$ refers to the raindrop-size distribution falling through a horizontal plane [5].

3. Building geometry and surrounding topography

Hunting Lodge St. Hubertus consists of a low-rise rectangular volume with wings that stretch out diagonally and with a characteristic tower in the middle of the building of 34.5 m height (Figs. 1a and 2). From the fourth floor up, the tower has a rectangular floor plan with dimensions 4.8 x 4.2 m^2. The outer parts of the south-west facade of the tower shaft, from the third till the seventh floor, are recessed compared to the middle part of this facade (Fig. 2a) Narrow recessed windows are present in the middle part. A loggia is present on each corner of the top floor of the tower. Furthermore, the tower is equipped with a chimney on the north-east side, and has a pitched roof.

The building is located at the northern side of the Dutch National Park "De Hoge Veluwe", longitude 52°07' and latitude 5°49', at approximately 42 m above sea level. The highest point in the area is found near Rheden, at 110 m above sea level. Rheden is situated 15 km south-east of the Hunting Lodge. The North Sea coast is about 100 km westwards of the park. Figure 3 shows an aerial view of the surroundings. There are no other buildings in the immediate vicinity of the Hunting Lodge. It is however surrounded by a forest. An elongated clear-cut in the forest is present south-west of the building, with a large pond, situated directly south-west of it.

4. Field measurements

The measurements of wind speed, wind direction, horizontal rainfall intensity and WDR were conducted at the building site from May until November 2007. All data were gathered on a 1-minute basis and were afterwards averaged over a time interval of 10 minutes. This choice is based on the results of a study by Blocken and Carmeliet [16], the conclusion of which was that high-resolution data (e.g. 10-minute data) should be used for accurate WDR calculations.

4.1 Wind

A meteorological mast was positioned at the north-west side of the building, in the middle between the building and the forest (position 1, Fig. 4). This position was chosen to minimise the influence of the building and its immediate surroundings on the measurements for south-west wind. The meteorological mast was equipped with an ultrasonic anemometer which provided measurements of the reference wind speed U_{10} (m/s) and the reference wind direction φ_{10} (degrees from north) at a height of 10 m. Comparison of the measured wind directions with meteorological data from the KNMI (Royal Netherlands Meteorological Institute) at a meteorological station nearby showed that the measurement of the wind direction was disturbed by the presence of the forest. A numerical simulation of the wind-flow pattern around the Hunting Lodge in which the surrounding forest was included confirmed this effect [24]. The trees with a height of approximately 20 m disturbed the measurement of the reference wind direction at 10 m height. The measurement of the wind direction was however correct when the wind was approaching from south-west (the prevailing direction in the Netherlands), because of the open area on that side of the building (Fig. 3). The disturbed measurement of the reference wind direction is one of the reasons why, for validation of the numerical model, only rain events with south-west wind during rainfall have been selected.

4.2 Rain

Horizontal rainfall was measured by a rain gauge with a horizontal orifice and a tipping-bucket mechanism. The measurement was conducted near the meteorological mast (Fig. 4). The wind error is the most important error that can occur during measurements of the horizontal rainfall intensity [25]. It refers to the deformation of the wind-flow pattern and the raindrop trajectories near the gauge orifice due to the presence of the gauge body. Therefore, in this study, a shield was placed around the rain gauge to minimize the wind error by reducing the upward wind-velocity vectors near the gauge orifice. Another important error originates from the rest water that stays behind in the tipping bucket after rain [20]. The maximum rest water error is the content of the tipping bucket, 2 ml in this study, which corresponds to 0.1 mm of horizontal rainfall.

4.3 Wind-driven rain

The measurement of WDR on the facades of the tower was performed with WDR gauges containing a tipping-bucket mechanism to register the amount of WDR. In this study, existing WDR gauges were redesigned based on the guidelines from an earlier study [10] and were manufactured at Eindhoven University of Technology (Fig. 5). The collection area of the WDR gauges is 0.2 x 0.2 m^2. Ordinary sheet glass was used for the collection area and for the draining tube to limit the amount of adhesion water [10]. The height of the rim of the gauges was only 10 mm to reduce the wind error. Furthermore, the rest-water error was limited by designing tipping buckets with a content of only 0.6 ml. This corresponds to 0.015 mm of WDR for the 0.2 x 0.2 m² collection area of the WDR gauge. The WDR gauge measurement resolution is therefore more than six times higher than the typical tipping-bucket resolution in standard (horizontal) rain gauges.

The positions at the facades and the numbers of the WDR gauges are given in Figure 2a. Most gauges were positioned at the south-west facade, because the prevailing wind direction in the Netherlands is south-west and most damage is observed at this facade. The WDR gauges were spread over the height and width of the south-west facade to gain insight in the spatial distribution of WDR. No measurements were performed at position 3, because of the difficulty to reach this position for attaching the gauge to the facade. The south-east, north-east and north-west facade of the tower were each equipped with one WDR gauge in the middle of the facade at the height of the balconies of the top floor, comparable to position 2 at the south-west facade.

5. Numerical wind-driven rain simulation

The WDR measurements at the few discrete positions do not give enough information to obtain a complete picture of the spatial distribution of WDR on the south-west facade of the tower. Therefore, they are supplemented with numerical simulations. The numerical method for simulation of WDR on buildings was developed by Choi [12,13] and extended by Blocken and Carmeliet [15,16]. It consists of five steps:

1. The steady-state wind-flow pattern around the building is calculated using RANS CFD.
2. Raindrop trajectories are obtained by injecting raindrops of different sizes in the calculated wind-flow pattern and by solving their equations of motion.
3. The specific catch ratio is determined based on the configuration of the calculated raindrop trajectories.
4. The catch ratio is calculated from the specific catch ratio and from the horizontal raindrop-size distribution.
5. From the data in step 4, catch-ratio charts are constructed for different positions at the building facade. The experimental data record of reference wind speed, reference wind direction and horizontal rainfall intensity for a given rain event is combined with the appropriate catch-ratio charts to determine the corresponding spatial and temporal distribution of WDR on the building facade. For more information on this step, the reader is referred to [15,16].

5.1 Building geometry, computational domain and grid

A computational domain with dimensions L X B X H = 350 x 350 x 205 m^3 is selected (Fig. 6). The blockage ratio (cross-sectional area of the building divided by the cross-sectional area of the domain) is about 0.7%. Two different building models have been used to determine the influence of the level of including geometrical facade details on the simulation results. The building geometry was simplified for the initial simulation to limit the computational cost (Fig. 7a). An unstructured mesh with tetrahedral cells was generated for this model, based on grid-sensitivity analysis with use of three different grids with a linear refinement factor $\sqrt{2}$. The analysis indicated that the grid with a total of 650,000 cells was appropriate. A part of this initial grid is shown in Figure 7c.

It is expected that simplification of the building geometry will provide an underestimation of the wind speed at the measurement positions 5 and 6 near the openings that are present above the parapets of the loggias (Fig. 2a), which are not included in the simplified model. The underestimation of the local wind speed would cause an underestimation of the local WDR intensity (catch ratios). To investigate this, a second building model was created. This model includes the details of the loggias on the corners of the top floor of the tower. It also includes the open spaces that are present behind the WDR gauges on the lower part of the tower shaft due to the recession of the windows and the recession of the outer facade parts (Fig. 7b). The unstructured mesh for this building model was again generated based on grid-sensitivity analysis. Three grids were constructed, a basic grid and a coarser and finer grid (linear refinement factor $\sqrt{2}$). The results of the mean wind speed from the different grids are compared along two horizontal lines and along one vertical line (Figs. 8a and 8b). The lines are chosen in front of the south-west facade of the tower (0.5 m from the surface), since the raindrops will travel through this area before impinging on the facade. Differences in mean wind speed close to the south-west facade will lead to different results in catch ratio. The horizontal lines are chosen at a height of 29 m, because this is the height where the building model is refined by including the loggias in the model. The results on different grids are compared with each other in Figures 8c-e, in terms of the horizontal, lateral and vertical velocity components, normalized by the reference wind speed U_{10}. No large differences can be observed between the solutions on the

different grids. The finest grid with a total of 2,110,012 cells has been used for further study because some minor differences are found between the results along rake 3 (Fig. 8e).

5.2 Boundary conditions

The boundary conditions represent the influence of the surroundings that are cut off by the computational domain (Fig. 6). The inlet of the domain is defined as a velocity inlet. The definition of the approach-flow profile of the mean wind speed that is imposed at the inlet is explained in the next section (5.2.1). Symmetry is prescribed at the top and at both sides of the domain. A constant static pressure of 0 Pa (relative to the operating pressure: 101320 Pa) is used at the outflow boundary. The standard wall functions by Launder and Spalding [26] with appropriate ground roughness specification [21] are used at the bottom of the domain.

5.2.1 Approach-flow profile of the mean wind speed

The approach-flow profile of the mean wind speed imposed at the inlet should be representative of the roughness characteristics of the upstream part of the domain that is cut off by the inlet plane [21]. This is expressed by the presence of the appropriate aerodynamic roughness length y_0 of this terrain in the expression of the logarithmic inlet profile of mean wind speed:

$$U(y) = \frac{u^*_{ABL}}{\kappa} \ln\left(\frac{y + y_0}{y_0}\right) \tag{2}$$

where U(y) is the mean streamwise wind speed at height y (m) above the ground plane (m/s), u^*_{ABL} the ABL friction velocity (m/s), κ the von Karman constant (0.42 in this study) and y_0 the aerodynamic roughness length (m). The ABL friction velocity is taken so that for the initial simulation a reference wind speed (U_{10}) of 10 m/s at a height of 10 m is obtained. The aerodynamic roughness length y_0 is visually estimated from aerial views of the surrounding terrain in combination with the updated Davenport roughness classification [22] (Table 1). A roughness length of 1 m represents a landscape that is totally and quite regularly covered with similar-size large obstacles, with open spaces comparable to the obstacle heights. This roughness length could be used to represent the terrain surrounding the Hunting Lodge, which is a rather dense forest with a height of approximately 20 m and some large open areas at larger distances.

Since some uncertainty exists in the estimation of the aerodynamic roughness length, two other values of y_0 have been used to determine the influence of this choice on the numerical results. A roughness length of 0.5 m represents an "old" cultivated landscape with many rather large obstacle groups separated by open spaces of about 10 obstacle heights. The description of a landscape with a roughness length of 2 m is "chaotic". This value is used to represent centres of large towns with a mixture of low-rise and high-rise buildings or irregular large forests with many clearings. Given these descriptions, the roughness length of the terrain surrounding the Hunting Lodge should be somewhere in between 0.5 and 2 m.

5.2.2 Approach-flow profiles of turbulence quantities

For y_0 = 1 m, the turbulence intensity I_u (-) is taken 31% at a height of 2 m and 8% at the top of the domain in this study. The turbulent kinetic energy k (m^2/s^2) is calculated from I_u (Eq. 3), assuming $\sigma_u^2 \approx \sigma_v^2 + \sigma_w^2$. The inlet profile of the turbulence dissipation rate ε(y) (m^2/s^3) is given by Equation 4.

$$k(y) = \frac{1}{2}(\sigma_u^2 + \sigma_v^2 + \sigma_w^2) \approx \sigma_u^2 = (I_u \cdot U(y))^2 \tag{3}$$

$$\varepsilon(y) = \frac{u^{*3}_{ABL}}{\kappa(y + y_0)} \tag{4}$$

5.2.3 Wall functions

The standard wall functions by Launder and Spalding [26] with the equivalent sand-grain roughness (k_S) modifications according to the formulae by Cebeci and Bradshaw are used. The roughness constant C_S is user defined in this study to obtain horizontal homogeneity, which means that the inlet profiles, the approach-flow profiles and the incident profiles are similar [21]. The required relationship between the equivalent sand-grain roughness height k_S (m), the aerodynamic roughness length y_0 (m) and the roughness constant C_S was derived by Blocken et al. [21] for Fluent 6.3:

$$k_s = \frac{9.793 \cdot y_0}{C_s} \tag{5}$$

The value of k_s is chosen as large as possible while satisfying the requirement that it should be smaller than the distance y_P from the centre point P of the wall-adjacent cell to the bottom of the domain [21]. The height of the wall-adjacent tetrahedral cells is 6 m, corresponding to a minimum y_P-value of about 1.5 m. The bottom of the domain is divided into nine sections to be able to model the roughness of the terrain surrounding the building properly. Figure 6 shows this division of the ground plane and the used values of k_s and C_S of each area. Note that k_S and C_S appear as a product in the roughness modification of the wall functions in Fluent 6.3 for aerodynamically rough walls. Therefore the individual values do not matter, as long as the product satisfies Eq. (5). With this is mind, the value of k_s is taken the same for all areas: 1.5 m. The roughness constant of the central and upstream area of the domain (forest clear-cut) is calculated from Equation 5, assuming $y_0 = 0.05$ m, yielding $C_S = 0.33$. The roughness constant for the other areas is also calculated using Equation 5, but with $y_0 = 1.0$ m, yielding $C_S = 6.53$.

5.3 Solver

The simulations of the steady-state wind-flow pattern were performed with the commercial CFD code Fluent 6.3 that employs the control-volume method. The wind-flow pattern around the Hunting Lodge is obtained by solving the Reynolds-Averaged Navier-Stokes (RANS) equations. This wind-flow pattern will be used to model the behaviour of raindrops impinging on the windward (south-west) facade of the tower. This is why the focus is mainly on the wind-flow pattern upstream of the building. The wind-flow pattern is calculated with the realizable k-ε model [27] and standard wall functions [26], based on results from earlier research [18]. Pressure-velocity coupling is taken care of by the SIMPLE algorithm. Pressure interpolation is second order. Second-order discretization schemes are used for both the convection terms and the viscous terms of the governing equations. The numerical simulation of the wind-flow pattern is performed for a reference wind speed $U_{10} = 10$ m/s. The wind-velocity vector fields for other reference wind speed values, needed for the tracking of raindrops, are obtained by linear scaling with U_{10}.

5.4 Numerical modelling of wind-driven rain

The raindrop trajectories are obtained by injecting raindrops of different sizes (diameters ranging from 0.5 to 1 mm in steps of 0.1 mm, from 1 to 2 mm in steps of 0.2 mm and from 2 to 6 mm in steps of 1 mm) in the calculated wind-flow pattern. Calculations of raindrop motions are conducted in flow patterns with U_{10} = 1, 2, 3, 5 and 10 m/s.

The south-west facade of the building is divided into small square zones of approximately 0.08 x 0.08 m^2 to obtain results with a high spatial resolution. The specific catch ratio is calculated for each zone, for all raindrop diameters and for each wind speed value. The catch ratios, integrated over all raindrop diameters, are calculated by adopting the raindrop-size distribution by Best [28], modified for horizontal rain fluxes as described in [5]. This raindrop-size distribution is a function of the horizontal rainfall intensity. For the calculation of the catch ratios, 16 values of horizontal rainfall intensity are used: 0, 0.1, 0.5, 1, 2, 3, 4, 5, 6, 8, 10, 12, 15, 20, 25 and 30 mm/h.

The last step of the numerical WDR simulation method consists of combining the results with the experimental data record of reference wind speed U_{10}, reference wind direction φ_{10} and horizontal rainfall intensity R_h for a given rain event. First, catch-ratio charts are constructed for each 0.08 x 0.08 m² position at the building facade, including those where the WDR measurements were performed. These three-dimensional charts show the catch ratio η as a function of U_{10} and R_h [15]. The spatial distribution of WDR on the south-west facade is determined for different rain events. These rain events have been selected carefully, to minimize measurement errors [11]. Only the results for two rain events are presented here.

5.4.1 Rain event 1

The record of U_{10}, φ_{10} and R_h during the rain event of September 17th, 2007 is given in Figure 9a. This rain event is composed of a few rain showers. The total horizontal rainfall amount S_h at the end of the rain event is 10.0 mm. The wind direction has generally been close to south-west (225° from north) during the rain event. The absolute WDR measurement error E_{wdr} is estimated following the procedure by Blocken and Carmeliet [10,11] and Nore et al. [20]. This error consists of the adhesion-water-evaporation error E_{AW} and the rest-water error E_{RW}. Other possible errors are expected to be of minor importance for this rain event. E_{AW} was estimated to be 0.2 mm and the rest-water error is 0.015 mm. The relative error estimate e_{wdr} at the end of the rain event is calculated for each measurement position and given in Table 2. Note that these estimates are very conservative [10,11,19], and that the actual errors are probably much smaller.

5.4.2 Rain event 2

The record of U_{10}, φ_{10} and R_h during the rain event of September 25th, 2007 is given in Figure 9b. S_h at the end of this rain event is 7.0 mm. The wind direction has been nearly south-west (225° from north) during the rain event. E_{AW} was estimated to be 0.06 mm and E_{RW} is 0.015 mm. The relative error e_{wdr} is given in Table 3. The measurement errors are much smaller for the second rain event, because there are less dry periods in the rain event during which adhesion-water evaporation can occur.

6. Results

6.1 Validation of the numerical model

The spatial distribution of the catch ratio at the end of both rain events is shown in Figure 10. The numerical results are those obtained with the detailed building model and with $y_0 = 1$ m. The experimental results are shown on the left-hand side of the figures, the numerical results on the right. The "classic" WDR wetting pattern is found [5]: wetting increases from bottom to top and from the middle to the sides. At the top of the facade, the differences between the simulations and the measurements, for the Sept. 17th rain event, are 30%, 14% and 21% at positions 2, 5 and 6, respectively (Fig. 10a). For the Sept. 25th rain event, the differences at these positions are 18%, 20% and 26%, respectively (Fig. 10b). Considering the complex nature of WDR and the large amount of influencing parameters, this can be considered a fair overall agreement between the experimental and the numerical results. Larger discrepancies however are found at position 4, where the catch ratios are underestimated by more than 50% by the simulations. This can be explained by Figure 11a. The raindrop trajectories ending at the lower part of the facade are bent away from the facade towards the vertical. This is especially the case for low wind speed (e.g., $U_{10} = 2$ m/s) in combination with the smaller raindrop diameters (e.g., d = 0.5 mm). Near the lower part of the facade, these raindrop trajectories are almost parallel to the facade, and do not always intersect with the surface, as shown in Figure 11a. Turbulent dispersion in the streamwise direction can cause these raindrops to deviate from their "mean" trajectory and to hit the facade anyway. Since turbulent dispersion is not modelled in this study, (more) rain will impinge on the lower part of the facade in reality than calculated with the numerical method. This statement is corroborated by an earlier study by Lakehal et al. [29] and by Figure 11b. Lakehal et al. [29] found that turbulent dispersion is an important factor increasing WDR on vertical walls in cases with weak upstream wind flow, such as in a street canyon. For the present study, Figure 11b displays the simulated profiles of the streamwise mean wind speed U and the streamwise turbulence intensity I_u ($= (2k/3)^{0.5}/U$) along a vertical line at a distance of 0.5 m from the facade, for $U_{10} = 2$ m/s. For the largest part of the facade, it indeed shows weak upstream wind flow ($U < 0.05$ m/s) and high turbulence intensity ($I_u > 100\%$), which are the conditions for which the conclusions of Lakehal et al. apply. Note that, apart from this effect, the calculation of the specific catch ratio at the lower part of the facade is considered less accurate due to the small intersection angle between the facade and the trajectories of those drops that do reach this lower part.

6.2 Influence of geometrical details

The calculated catch ratio values for both the initial and the detailed building model and their comparison with the experiments are shown in Figure 12. We focus on the top positions 2, 5 and 6, for which the simulations are considered most accurate. Figure 12a shows that including the facade details yields improvements of 0%, 14% and 8% for positions 2, 5 and 6, respectively. Figure 12b shows improvements of 4%, 11% and 6% for these positions. The improvements are clearly most pronounced at positions 5 and 6 near the details (loggias).

A more detailed comparison is performed by also focusing at the facade positions where no measurements were conducted. Therefore, the south-west facade was divided into different zones (Fig. 13a). The analysis is made for $U_{10} = 3$ and 10 m/s and $R_h = 2$ and 10 mm/h. Figures 13b and c compare the catch ratio obtained with the initial and the detailed model. Figure 13b shows that catch ratios increase for parts b, c and d (the parts of the facade surrounding the loggias) when the model with a higher level of geometrical detail is used. Increases for part d locally go up to 40%, and are clearly larger than those for part c. The catch ratios decrease for parts f2 and a section of part e. No conclusions can be drawn from these decreases since, as explained in section 6.1, the numerical results are less accurate for lower parts of the facade because turbulent dispersion is neglected. The differences at the other positions are generally within 10%. The rainfall intensity has no clear influence on the differences.

For higher wind speeds, the catch ratios obtained with the detailed model are within the range of +10% and -10% of the catch ratios calculated with the initial model, for all parts of the facade and for both high and low rainfall intensities (Fig. 13c). For parts b, c and d, the absolute differences are comparable to those found for low wind speeds, but are relatively less pronounced because the catch ratios are larger for high wind speeds.

The representation of geometrical details significantly influences the numerical results for those parts of the facade surrounding the loggias on the top floor of the tower, at least for low wind speed ($U_{10} = 3$ m/s) and for both high and low rainfall intensities.

6.3 Influence of the approach-flow profile

Simulations of wind and WDR are also made with two additional aerodynamic roughness lengths, $y_0 = 0.5$ m and $y_0 = 2$ m. The inlet profiles of mean wind speed and turbulence quantities are adjusted to these values. The ground roughness in the computational domain (Fig. 6) is kept the same. The inlet mean wind speed profiles for the three different y_0 values are shown in Figure 14a. Note that these profiles are matched at the height of the loggias and the measurement positions 2, 5 and 6: see Figure 2a. It logically implies that the differences in mean wind speed between the different profiles are less pronounced around this height. This is reflected in the WDR simulation results, shown in Figure 15. We focus on positions 2, 5 and 6. Except for position 2 in Figure 15a, the changes in catch ratio by changing y_0 from 0.5 m to 1 m and to 2 m are less than 10%. This might lead to the conclusion that the choice of y_0 is not that critical for WDR studies. However, it should be noted that this conclusion holds for this particular case, for these positions, and, more importantly, when the profiles are matched at 29 m height. If the profiles are matched at e.g. 10 m height, the differences between these profiles are much more pronounced near the top of the tower (Fig. 14b). Because the reference wind speed is usually measured at 10 m height, as in this study, this will be the height at which the "numerical" inlet profile will be matched to the measured mean wind speed value. Therefore, an incorrect choice of y_0 will probably have an important influence on the results.

7. Discussion

7.1 Accuracy of the measurements

Given the large errors that can occur in horizontal rain and WDR measurements [3,9-11], specific attention was paid to measurement accuracy. The measurement error of the WDR gauges is minimized by adhering to guidelines for the design of these gauges [10]. The amount of adhesion water at the gauge collection area is limited by choosing an appropriate gauge material (plain sheet glass – see [10]). The amount of adhesion water in the draining tube is limited by keeping the tube as short as possible and by constructing the tube of glass. The height of the rim of the gauge is limited to reduce wind errors and the content of the tipping buckets is limited to reduce the rest-water error. The accuracy of the measurement of the horizontal rainfall intensity was improved by placing a wind screen around the rain gauge to reduce the wind error. Furthermore, attention has been paid to positioning the meteorological mast and the horizontal rain gauge to minimise the influence of the buildings and its immediate surroundings on the measurements for south-west wind.

Although the measurements have been conducted for seven months, only a limited amount of rain events can be used for the WDR validation study, due to the strict character of the guidelines for the selection of accurate and reliable experimental WDR data [11]. There are two reasons why only rain events have been used where the wind direction has generally been perpendicular to the south-west facade (225° from north). The first reason is that the wind error in the WDR measurements is expected to be less important for these rain events. The second reason is the ascertained influence of the surrounding forest on the measurement of the reference wind direction. For simplicity, the trees have not been modelled for calculation of the wind-flow pattern used for the WDR simulations. The measurement of the wind direction appeared to be only correct when wind is approaching from south-west. For all other wind directions, the local wind direction at the measurement location deviates from the wind direction above the forest. This is due to the channeling of wind in the corridor that consists of the elongated forest clear-cut with the pond (Fig. 3). This effect was demonstrated by performing CFD simulations (wind only, not WDR) for situations with and without the trees present, and for south-west and west wind directions [24]. Note that Fig. 9 shows that the measured wind directions are slightly lower than 225°. This is the reason for the higher catch ratio at position 6 than at position 5 in Fig. 10. This asymmetry is not found for the numerical catch ratios, because simulations were only performed for 225°. Detailed information on the sensitivity of WDR exposure to the wind direction can be found in [19,30]. Finally, the measurement accuracy has also been enhanced by selecting rain events with high amounts of WDR and few interruptions of the rainfall to limit the adhesion-water-evaporation error. The influence of splashing is expected to be small for all rain events because of the low wind-speed values during these events.

7.2 Accuracy of the numerical simulations

The accuracy of the numerical simulations is determined by the accuracy of the calculated wind-flow pattern, the accuracy of the calculated raindrop trajectories and the accuracy of the meteorological input data.

For the calculation of the wind-flow pattern, the uncertainty in the estimation of the roughness of the surrounding terrain has been analysed by calculation of catch ratios with the use of different roughness lengths in the definition of the approach-flow profile of the wind speed. A more detailed study however should be performed with profiles that are matched at the measuring height (10 m) of the reference wind speed and direction.

Two assumptions have been made for the numerical modelling of wind-driven rain. The raindrop-size distribution by Best [28] has been adopted for determination of the numerical catch ratios. Although this formula is based on an extensive study for a large number of rain events, deviations from the spectra are likely to occur.

Blocken and Carmeliet [15] showed though that the variation of the specific catch ratio with drop size is limited to the smaller drop sizes and that their specific catch ratio does not have a large contribution to the overall catch ratio for moderate to high rainfall intensities. This might indicate that the sensitivity to raindrop spectra is rather small. Furthermore, turbulent dispersion was not modelled. It has appeared that in the situation under study, accurate results can be obtained without including turbulent dispersion for upper parts of the facade. However, turbulent dispersion may probably not be neglected for lower parts of the facade.

The accuracy of the meteorological input data is determined by the accuracy of the measurements of the reference wind speed, the reference wind direction and the horizontal rainfall intensity. The sample size of these data is of high importance. Using hourly wind and rain data can lead to very large errors in WDR calculations [16]. Therefore, high-resolution data were used in this study (1-minuta data converted to 10-minute average values).

8. Conclusions

CFD simulations of wind-driven rain (WDR) on the south-west facade of a monumental building tower have been performed. The simulations have been compared with full-scale measurements and a sensitivity analysis has been conducted concerning the level of geometrical facade detailing and the upstream terrain aerodynamic roughness length. The following conclusions are made:

The numerical and the experimental results have been compared in terms of the catch ratio value at the end of each rain event. At the upper part of the south-west tower facade, the differences between the catch ratio values range from 14% to 30%. Given the complex nature of WDR and the large number of influencing parameters, this is considered a fair agreement. Larger discrepancies however have been observed at the lower position, where the simulations underestimate the amount of WDR by more than 50%. This underestimation is mainly attributed to the turbulent dispersion of the raindrops, which is not included in the model. This is considered particularly important for the lower part of the facades of high-rise buildings.

Including the facade details yields significant improvements (up to 14%) at the measurement positions 5 and 6, which are in the direct vicinity of these details. A more detailed comparison shows that very close to the details i.e. just below the openings at the loggias on the top floor of the tower, catch ratios increase by 40% for U_{10} = 3 m/s. The effect of the details is less pronounced for higher wind speeds (U_{10} = 10 m/s). No conclusions can be drawn for lower parts of the facade due to the fact that turbulent dispersion was neglected, and modelling accuracy is low at these locations.

When the different inlet mean wind-speed profiles are matched at the height of interest, the WDR simulation results at this height appear quite insensitive (differences less than 10%) to changes in upstream aerodynamic terrain roughness length y_0 from 0.5 m to 1 m and 2 m. However, wind speed measurements are often conducted at 10 m height and this will generally be the matching height. In that case, changes will probably be significant and a correct estimate of y_0 is important.

These conclusions apply to the present situation of building and surroundings. More research is needed to expand the validity of these findings.

Acknowledgements

This research is funded by the Dutch Government Building Agency. Their financial contribution is gratefully acknowledged. The authors wish to express their gratitude for the kind assistance and hospitality of the managers of the Hunting Lodge and the staff of the National Park “De Hoge Veluwe”. Appreciation is also expressed to the staff of the Laboratory of the Unit Building Physics and Systems (BPS) of Eindhoven University of Technology for their valuable assistance in the design and installation of the measurement set-up.

Nomenclature

C_S	roughness constant (-)
d	raindrop diameter (mm)
E_{AW}	absolute adhesion-water-evaporation error (mm)
E_{RW}	absolute rest-water error (mm)
E_{wdr}	absolute WDR measurement error (mm)
e_{wdr}	relative WDR measurement error (= E_{wdr}/S_{wdr}) (-)
$f_h(d)$	probability-density function of raindrop size falling through a horizontal plane (m^{-1})
I_u	turbulence intensity (-)
k	turbulent kinetic energy (m^2/s^2)
k_s	physical roughness height (m)
L, B, H	length, width and height of the computational domain (m)
R_h	horizontal rainfall intensity, i.e. through a horizontal plane (L/m^2h of mm/h)
R_{wdr}	wind-driven rain intensity (L/m^2h of mm/h)
S_h	horizontal rainfall amount, i.e. through a horizontal plane (L/m^2 or mm)

S_{wdr}	wind-driven rain amount (L/m^2 or mm)
u^*_{ABL}	friction velocity associated with the inlet profiles of U, k and ε (m/s)
U, V, W	streamwise, vertical and lateral component of the mean wind-velocity vector (m/s)
U_{10}	reference wind speed at 10 m height in the upstream undisturbed flow (m/s)
U(y)	mean streamwise wind speed at height y (m) above the ground plane (m/s)
y	height co-ordinate (m)
y_0	aerodynamic roughness length (m)
y_P	distance from the centre point P of the wall-adjacent cell to the wall (m)
ε	turbulence dissipation rate (m^2/s^3)
η_d	specific catch ratio (-)
η	catch ratio (-)
κ	von Karman constant (≈ 0.42)
φ_{10}	reference wind direction at 10 m height in the upstream undisturbed flow (degrees from north)
ABL	Atmospheric Boundary Layer
CFD	Computational Fluid Dynamics
HAM	Heat-Air-Moisture
RANS	Reynolds-Averaged-Navier-Stokes (equations)
WDR	Wind-Driven Rain

References

[1] Hens H. Heat, air and moisture transfer in insulated envelope parts: modelling. International Energy Agency, Annex 24. Final report, volume 1. Leuven: Acco; 1996.

[2] Sanders C. Heat, air and moisture transfer in insulated envelope parts: Environmental conditions. International Energy Agency, Annex 24. Final report, volume 2. Leuven: Acco; 1996.

[3] van Mook FJR. Driving rain on building envelopes. PhD thesis. Building Physics Group (FAGO), Eindhoven University of Technology, The Netherlands, 2002.

[4] Dalgliesh WA, Surry D. BLWT, CFD and HAM modelling vs. the real world: Bridging the gaps with full-scale measurements. Journal of Wind Engineering and Industrial Aerodynamics 2003; 91(12-15): 1651-1669.

[5] Blocken B, Carmeliet J. A review of wind-driven rain research in building science, Journal of Wind Engineering and Industrial Aerodynamics 2004; 92(13): 1079-1130.

[6] Blocken B, Roels S, Carmeliet J. A combined CFD-HAM approach for wind-driven rain on building facades. Journal of Wind Engineering and Industrial Aerodynamics 2007; 95(7): 585-607.

[7] Janssen H, Blocken B, Carmeliet J. Conservative modelling of the moisture and heat transfer in building components under atmospheric excitation. International Journal of Heat and Mass Transfer 2007; 50 (5-6): 1128-1140.

[8] Abuku M, Janssen H, Poesen J, Roels S. Impact, absorption and evaporation of raindrops on building facades, Building and Environment 2008. In Press, (doi:10.1016/j.buildenv.2008.02.001).

[9] Högberg AB, Kragh MK, van Mook FJR. A comparison of driving rain measurements with different gauges. In: Proceedings of the fifth symposium of building physics in the Nordic countries, Göteborg, Sweden, 1999, pp. 361-368.

[10] Blocken B, Carmeliet J. On the accuracy of wind-driven rain measurements on buildings. Building and Environment 2006; 41(12): 1798-810.

[11] Blocken B, Carmeliet J. High-resolution wind-driven rain measurements on a low-rise building—experimental data for model development and model validation. Journal of Wind Engineering and Industrial Aerodynamics 2005; 93(12): 905-28.

[12] Choi ECC. Simulation of wind-driven rain around a building. Journal of Wind Engineering and Industrial Aerodynamics 1993; 46&47: 721-729.

[13] Choi ECC. Determination of wind-driven rain intensity on building faces. Journal of Wind Engineering and Industrial Aerodynamics 1994; 51: 55-69.

[14] Choi ECC. Parameters affecting the intensity of wind-driven rain on the front face of a building. Journal of Wind Engineering and Industrial Aerodynamics 1994; 53: 1-17.

[15] Blocken B, Carmeliet J. Spatial and temporal distribution of driving rain on a low-rise building. Wind and Structures 2002; 5(5): 441–62.

[16] Blocken B, Carmeliet J. On the errors associated with the use of hourly data in wind-driven rain calculations on building facades. Atmospheric Environment 2007; 41(11): 2335-2343.

[17] Tang W, Davidson CI. Erosion of limestone building surfaces caused by wind-driven rain. 2. Numerical modelling. Atmospheric Environment 2004; 38(33): 5601–5609.

[18] Blocken B, Carmeliet J. Validation of CFD simulations of wind-driven rain on a low-rise building facade. Building and Environment 2007; 42(7): 2530–2548.
[19] Abuku M, Blocken B, Nore K, Thue JV, Carmeliet J, Roels S. On the validity of numerical wind-driven rain simulation on a rectangular low-rise building under various oblique winds. Building and Environment, 2008. In Press, (doi:10.1016/j.buildenv.2008.05.003).
[20] Nore K, Blocken B, Jelle BP, Thue JV, Carmeliet J. A dataset of wind-driven rain measurements on a low-rise test building in Norway. Building and Environment 2007; 42(5): 2150-2165.
[21] Blocken B, Stathopoulos T, Carmeliet J. CFD simulation of the atmospheric boundary layer: wall function problems. Atmospheric Environment 2007; 41(2): 238-252.
[22] Wieringa, J. Updating the Davenport roughness classification. Journal of Wind Engineering and Industrial Aerodynamics 1992; 41-44: 357-368.
[23] Choi ECC. Numerical modelling of gust effect on wind-driven rain. Journal of Wind Engineering and Industrial Aerodynamics 1997; 72: 107-116.
[24] Briggen PM. Investigation of the causes of moisture damage at the tower of Hunting Lodge St. Hubertus (In Dutch). Master Thesis, Building Physics and Systems, Eindhoven University of Technology, the Netherlands, 2007.
[25] WMO, World Meteorological Organization. Guide to meteorological instruments and methods of observation. 1996; WMO-No.8 (6).
[26] Launder BE, Spalding DB. The numerical computation of turbulent flows. Computer Methods in Applied Mechanics and Engineering 1974; 3: 269-289.
[27] Shih TH, Liou WW, Shabbir A, Zhu J. A new k-ε eddy-viscosity model for high Reynolds number turbulent flows – model development and validation. Computers and Fluids 1995; 24(3): 227-238.
[28] Best AC. The size distribution of raindrops. Quarterly Journal of the Royal Meteorological Society 1950; 76(327): 16-36.
[29] Lakehal D, Mestayer PG, Edson JB, Anquetin S, Sini JF. Eulero-Lagrangian simulation of raindrop trajectories and impacts within the urban canopy. Atmospheric Environment 1995; 29(23): 3501–3517.
[30] Blocken B, Carmeliet J. On the validity of the cosine projection in wind-driven rain calculations on buildings. Building and Environment 2006; 41(9): 1182-1189.

FIGURE CAPTIONS

Figure 1. (a) Hunting Lodge St. Hubertus and (b-e) moisture damage at the tower due to wind-driven rain: (b) salt efflorescence; (c) cracking/blistering due to salt crystallisation; (d) rain penetration and discolouration; (e) cracking at inside surface.

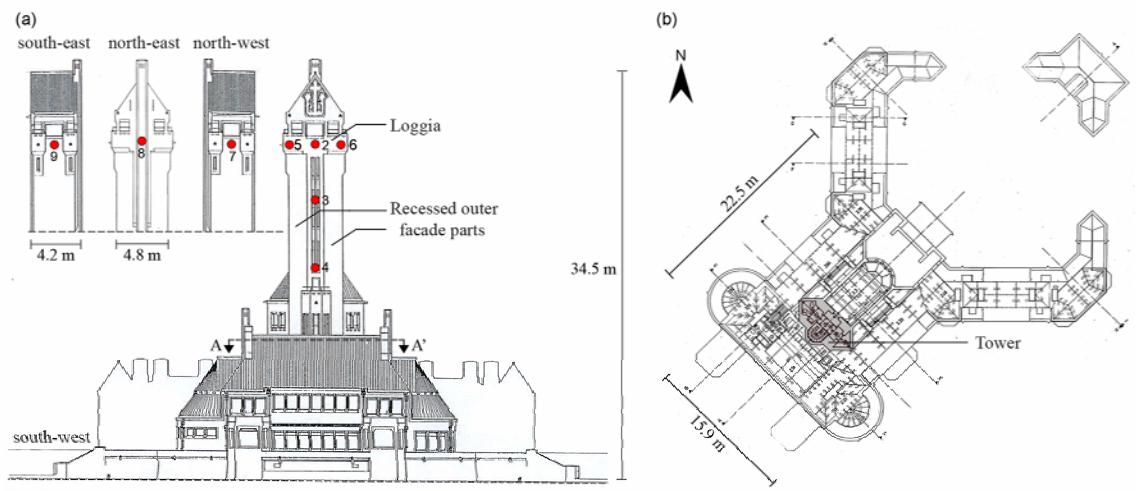

Figure 2. (a) Building dimensions and positions and numbers of the wind-driven rain gauges at the facades of the tower; (b) cross section A-A' (indicated in Fig. 2a) of the building.

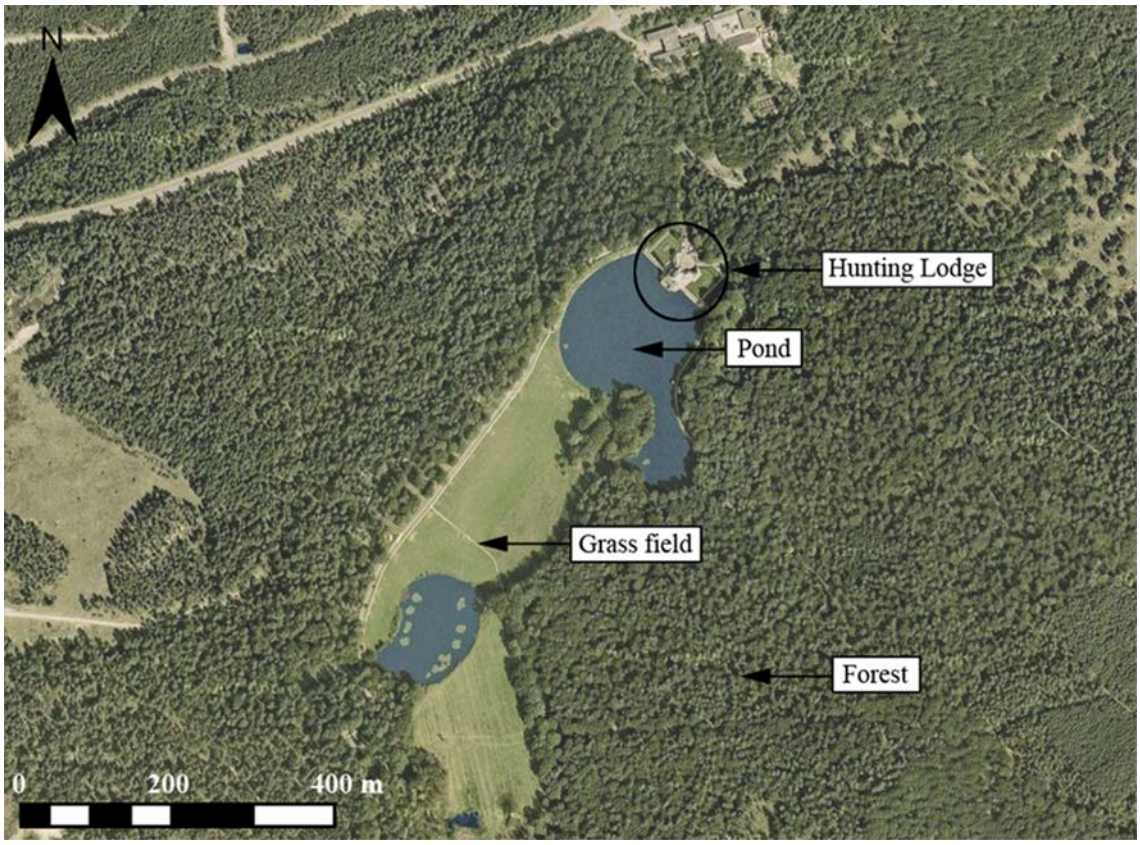

Figure 3. Aerial view of the topography surrounding the Hunting Lodge.

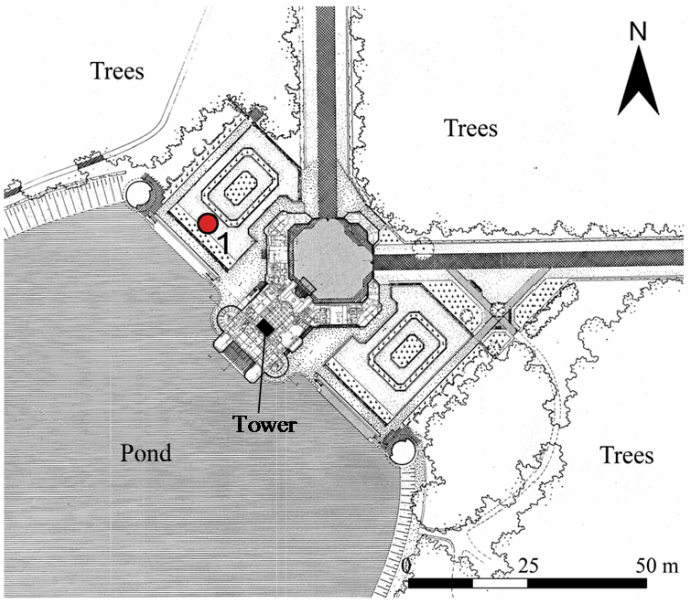

Figure 4. Position of the meteorological mast (measurement of reference wind speed and reference wind direction) and the horizontal rain gauge, both at position 1.

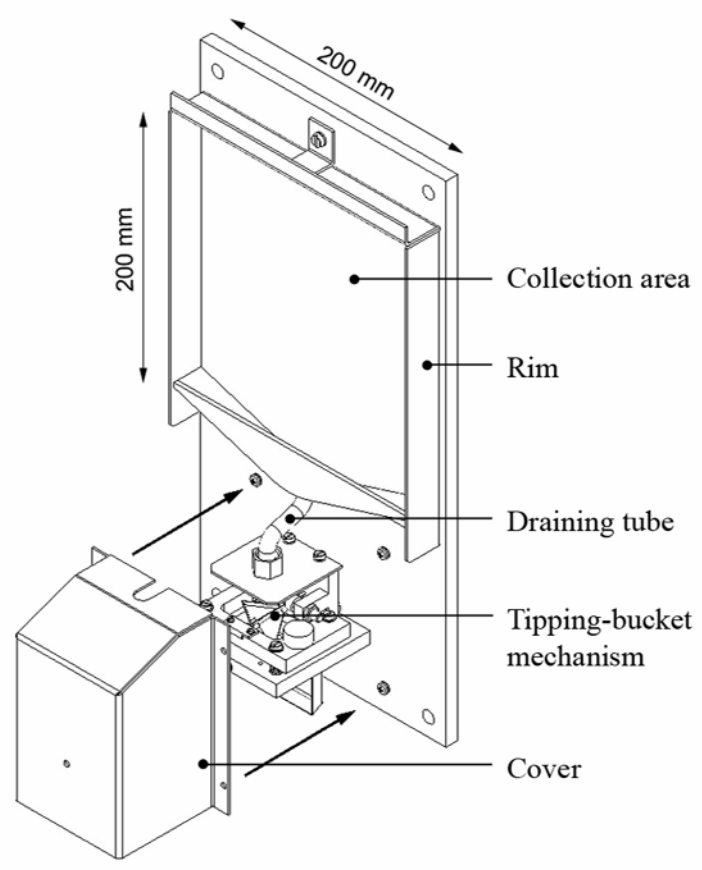

Figure 5. Wind-driven rain gauge, designed and manufactured at Eindhoven University of Technology.

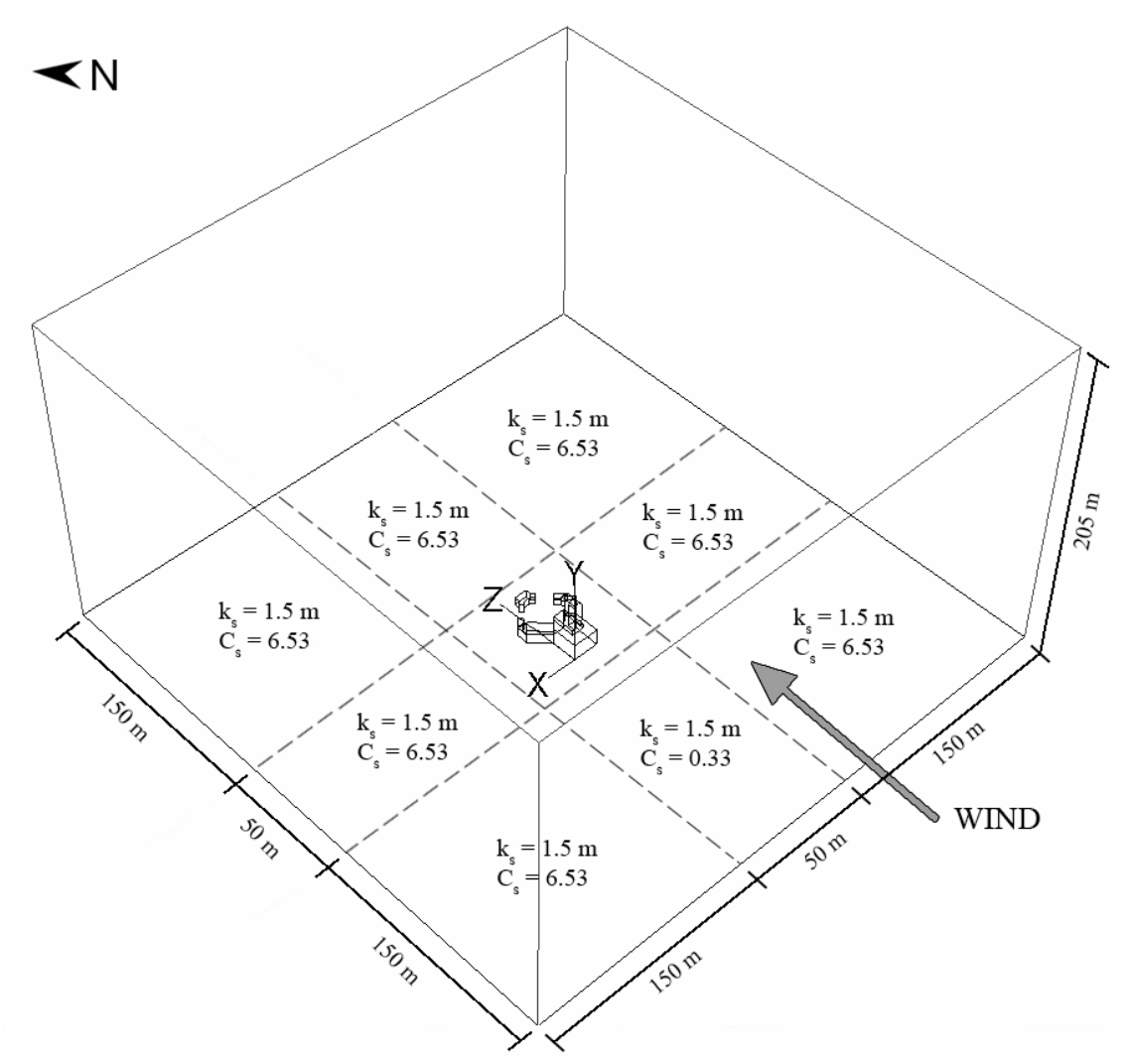

Figure 6. Computational domain and division of the ground plane with indication of the values of the physical roughness height k_s and the roughness constant C_S for each area (k_s = 1.5 m and C_S = 0.33 for the central area of the domain). Note that not the individual values, but the product $k_S C_S$ determines the roughness modification in the wall functions.

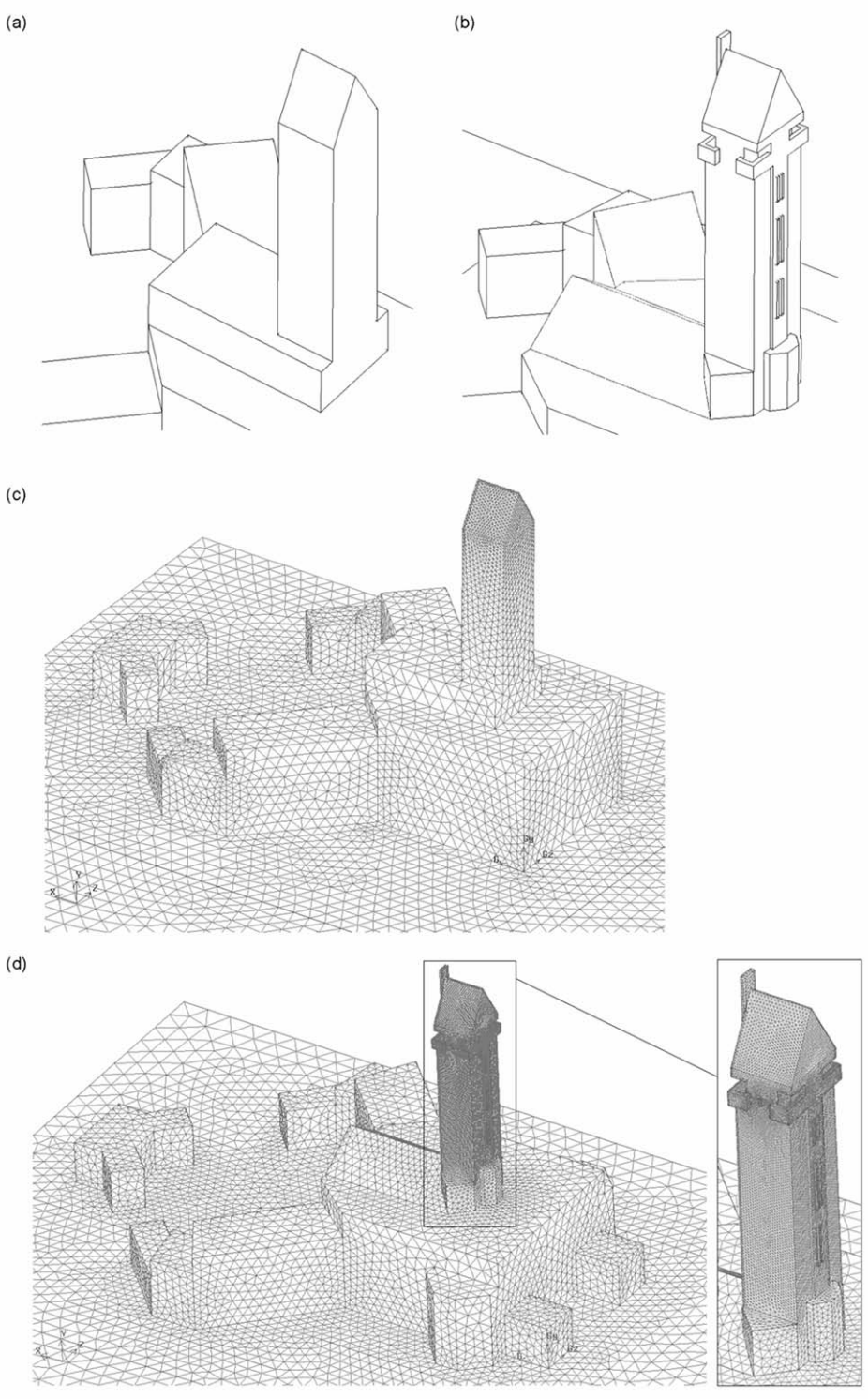

Figure 7. Part of the building models and surface grids used for calculation of the wind-flow pattern around the building. (a) Initial model; (b) detailed model; (c) grid used for the initial building model (650,000 cells); (d) grid used for the detailed building model (2,110,012 cells).

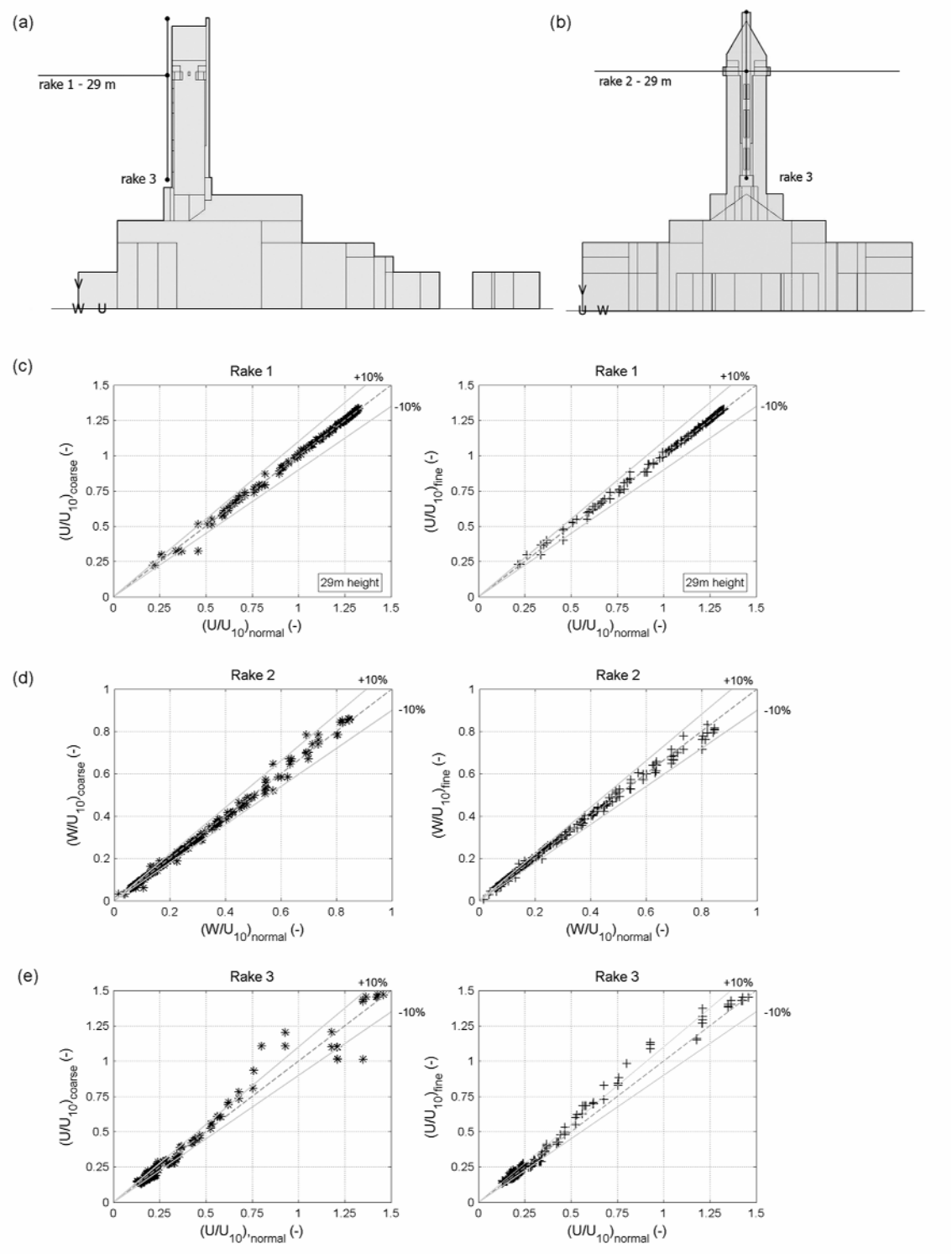

Figure 8. Grid-sensitivity analysis for the detailed building model by comparing results obtained on three different grids along three lines. (a) Positions of the horizontal line in x(U)-direction (rake 1) and the vertical line in y(V)-direction (rake 3); (b) positions of the horizontal line in z(W)-direction (rake 2) and the vertical line in y(V)-direction (rake 3); (c) comparison for dimensionless wind-speed component U/U_{10} along rake 1; (d) comparison for dimensionless wind-speed component W/U_{10} along rake 2; (e) comparison for dimensionless wind-speed component U/U_{10} along rake 3.

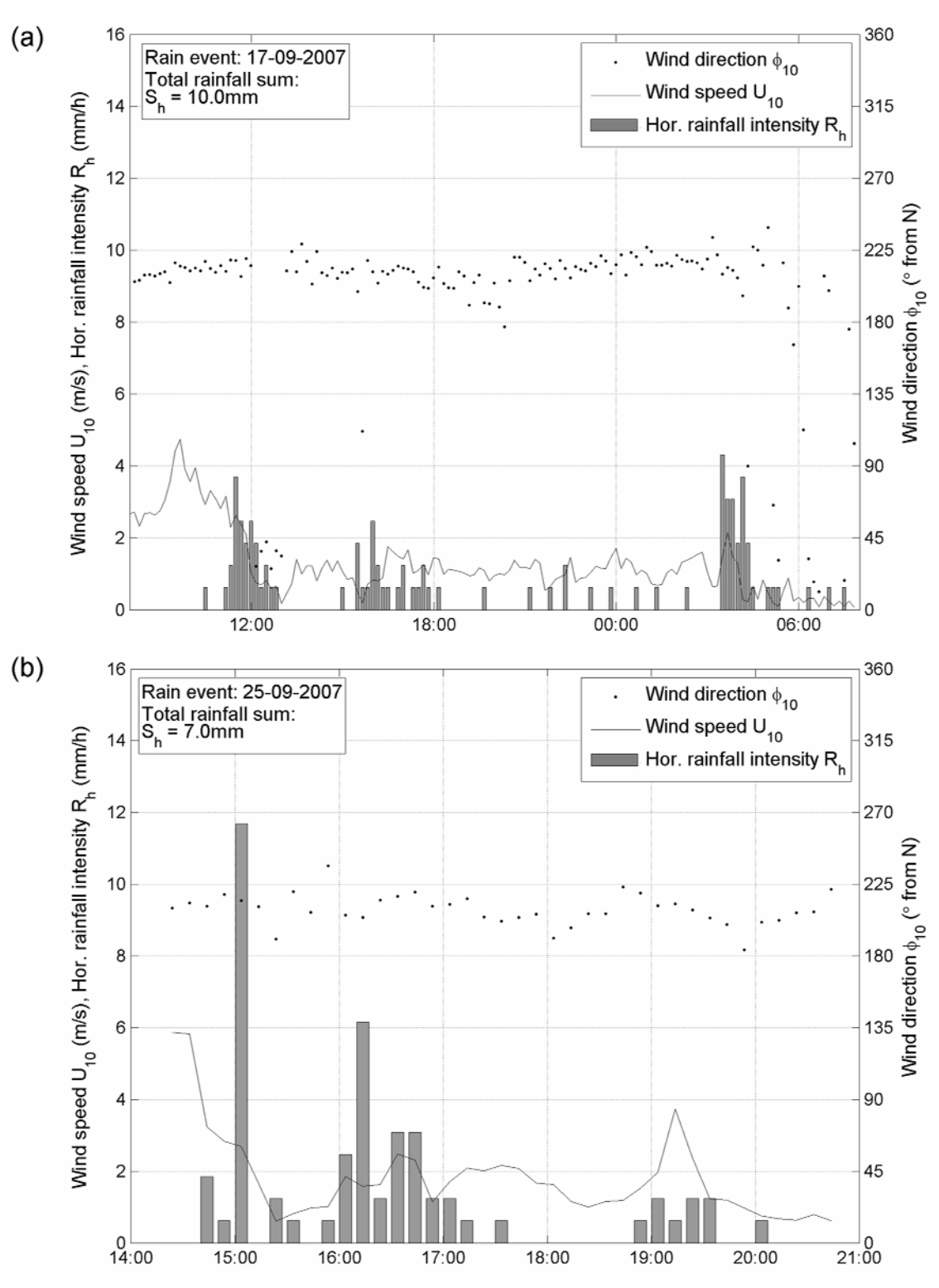

Figure 9. Record of the meteorological data (reference wind speed, wind direction and horizontal rainfall intensity) for two rain events. (a) September 17th, 2007; (b) September 25th, 2007.

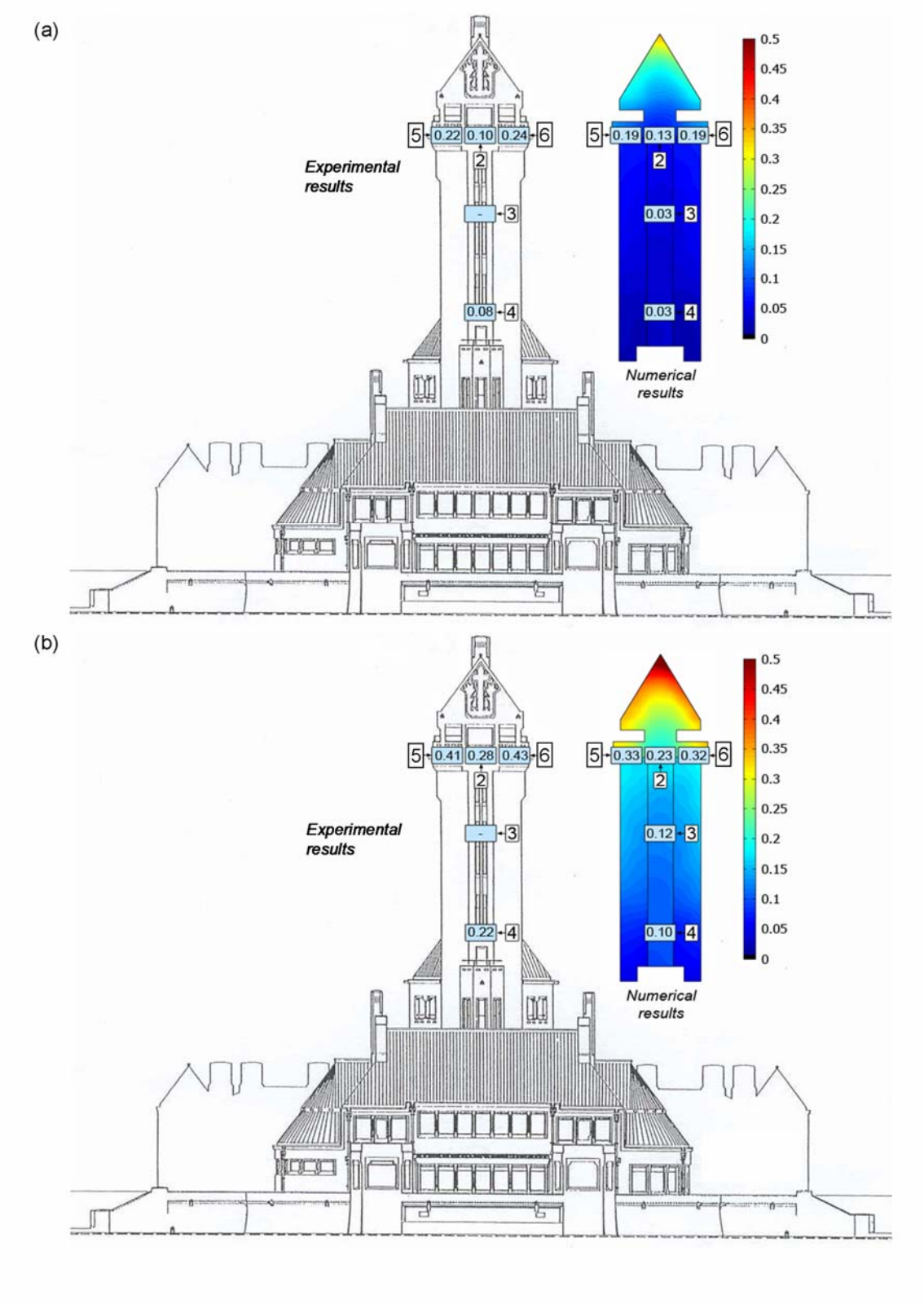

Figure 10. Spatial distribution of the catch ratio at the end of the two rain events. The experimental results at the locations of the wind-driven rain gauges are shown on the left, the numerical results are shown on the right. (a) September 17th, 2007; (b) September 25th, 2007.

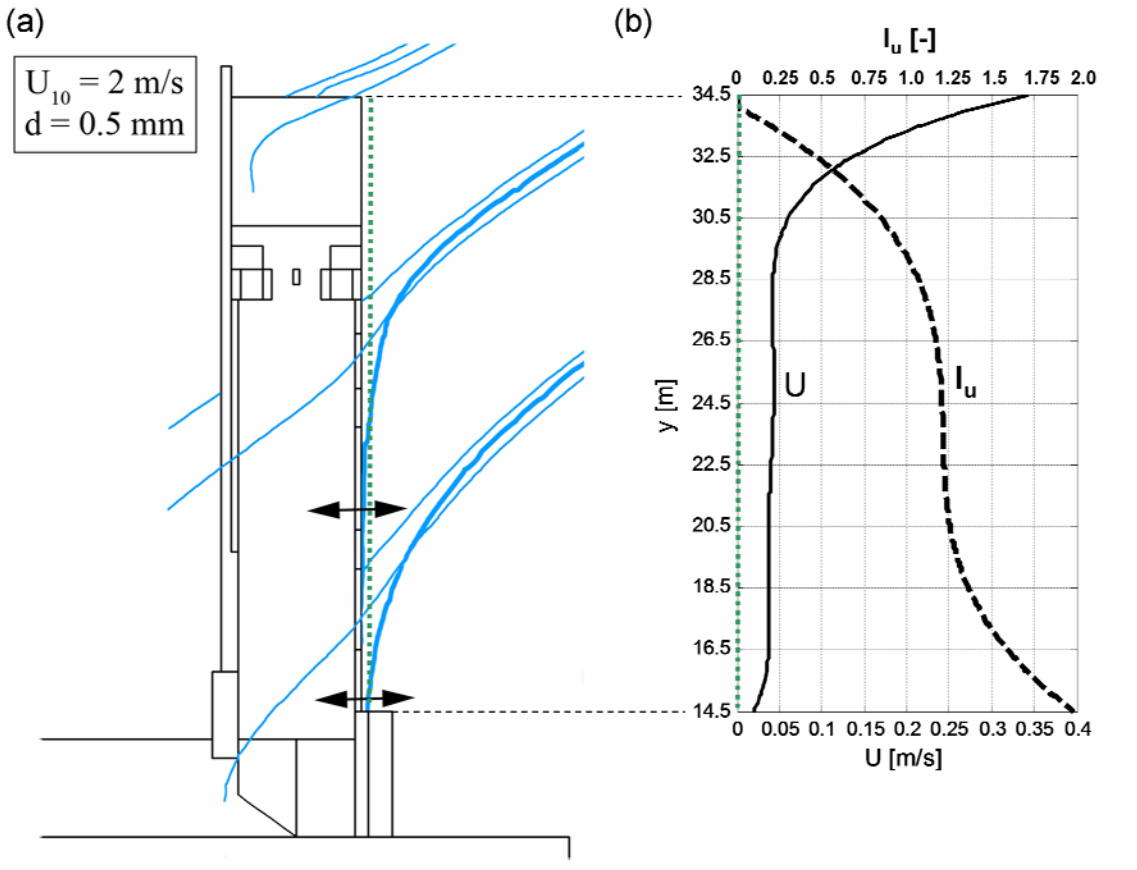

Figure 11. (a) Raindrop trajectories of d = 0.5 mm in the U_{10} = 2 m/s wind field. Turbulent dispersion in the streamwise direction (indicated by the arrows) can cause raindrops to hit the facade. (b) streamwise mean wind speed U and streamwise turbulence intensity I_u along a vertical line at a distance of 0.5 m from the windward facade.

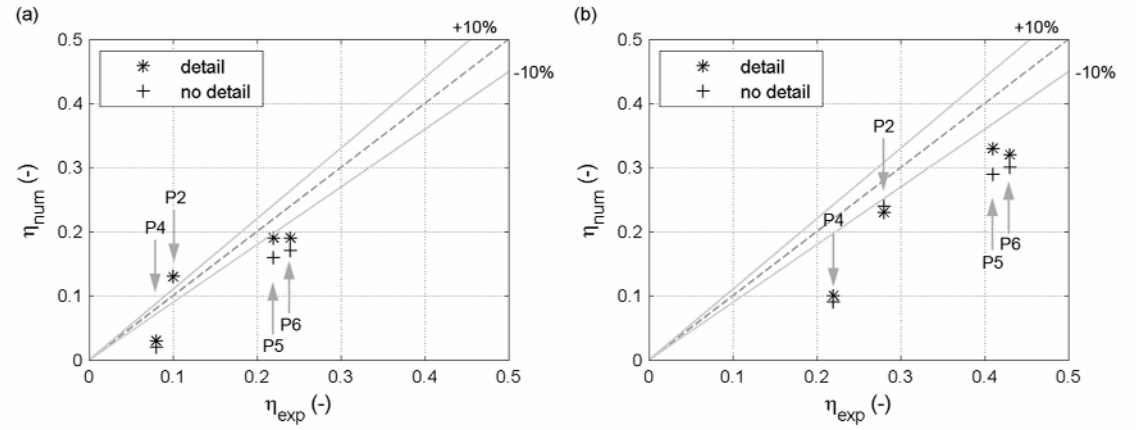

Figure 12. Comparison of numerical and experimental catch ratio values for the initial building model and for the detailed building model. (a) For the rain event of September 17th, 2007; (b) for the rain event of September 25th, 2007.

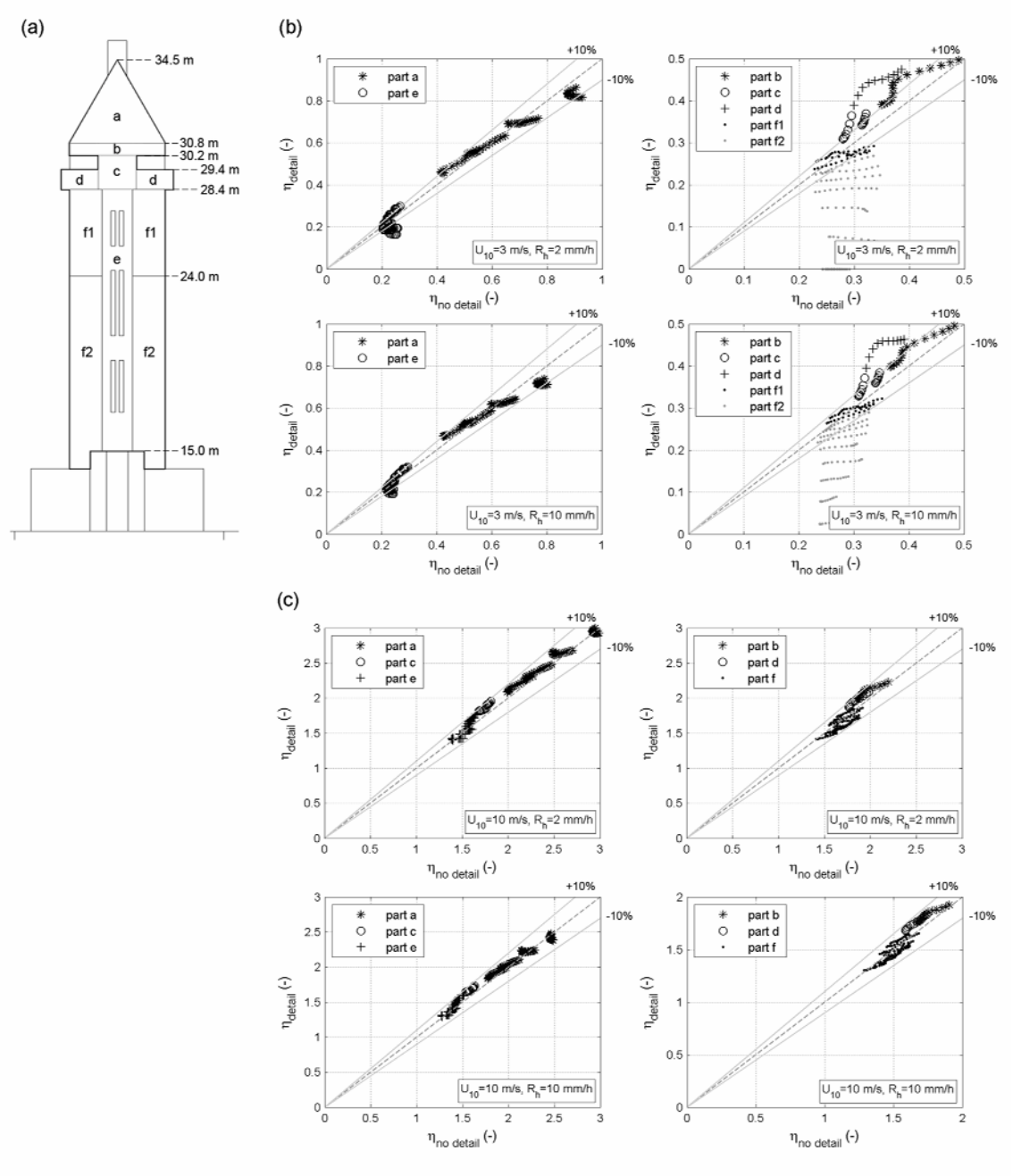

Figure 13. Comparison between the results of the simulation with the initial model and the detailed model. (a) Division of the south-west facade into zones; (b) results for U_{10} = 3 m/s; (c) results for U_{10} = 10 m/s.

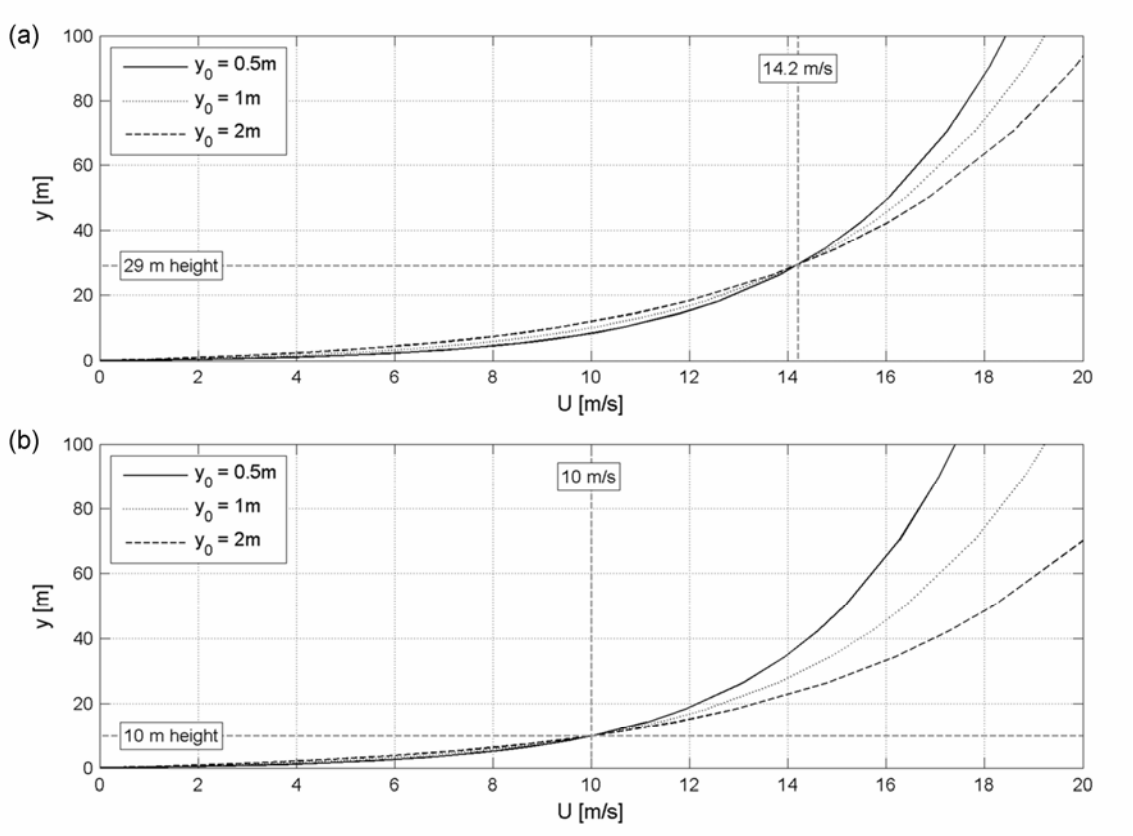

Figure 14. Approach-flow profiles of the mean wind speed with three different values of y_0. (a) Mean wind speed matched at a height of 29 m; (b) mean wind speed matched at a height of 10 m.

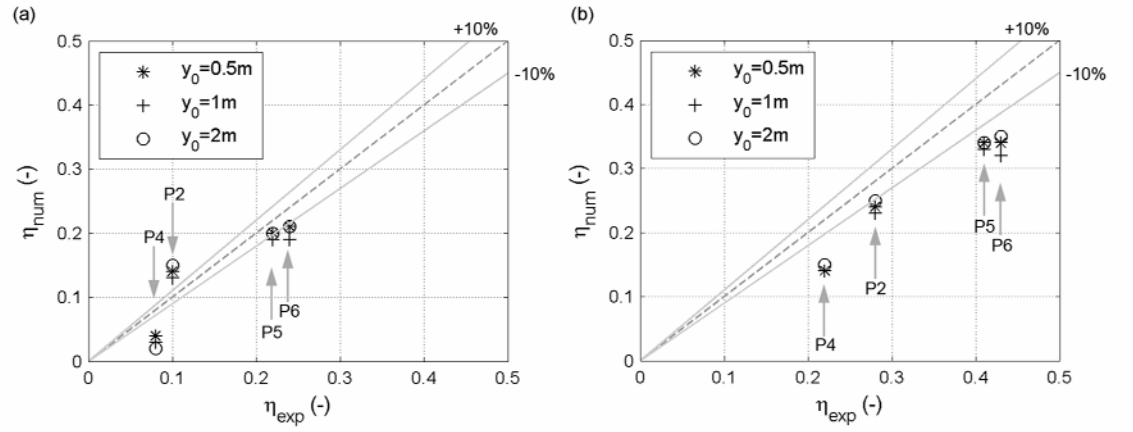

Figure 15. Comparison of numerical and experimental catch ratio values obtained with the different y_0 in the definition of the approach-flow profiles. (a) For the rain event of September 17th, 2007; (b) for the rain event of September 25th, 2007.

Table 1: Davenport classification of aerodynamic terrain roughness length as updated by Wieringa [22]. Values can be extracted from the table by a visual determination of the roughness class on condition that it is based on a fetch of at least 5 km.

	y_0 (m)	Landscape description
1	0.0002 Sea	Open sea or lake (irrespective of the wave size), tidal flat, snow-covered flat plain, featureless desert, tarmac, concrete, with a free fetch of several kilometres.
2	0.005 Smooth	Featureless land surface without any noticeable obstacles and with negligible vegetation; e.g. beaches, pack ice without large ridges, morass, and snow-covered or fallow open country.
3	0.03 Open	Level country with low vegetation (e.g. grass) and isolated obstacles with separations of at least 50 obstacle heights; e.g. grazing land without windbreaks, heather, moor and tundra, runway area of airports.
4	0.10 Roughly open	Cultivated area with regular cover of low crops, or moderately open country with occasional obstacles (e.g. low hedges, single rows of trees, isolated farms) at relative horizontal distances of at least 20 obstacle heights.
5	0.25 Rough	Recently-developed "young" landscape with high crops or crops of varying height, and scattered obstacles (e.g. dense shelterbelts, vineyards) at relative distances of about 15 obstacle heights.
6	0.50 Very rough	"Old" cultivated landscape with many rather large obstacle groups (large farms, clumps of forest) separated by open spaces of about 10 obstacle heights. Also low large vegetation with small interspaces such as bush land, orchards, young densely-planted forest.
7	1.0 Closed	Landscape totally and quite regularly covered with similar-size large obstacles, with open spaces comparable to the obstacle heights; e.g. mature regular forests, homogeneous cities or villages.
8	≥ 2.0 Chaotic	Centres of large towns with mixture of low-rise and high-rise buildings. Also irregular large forests with many clearings.

Table 2: Error estimates for the accumulated wind-driven rain measured at the south-west facade for the rain event of September 17th, 2007.

WDR gauge	S_{wdr} (mm)	E_{wdr} (mm)	e_{wdr} (%)
P2	1.0	0.22	22.0
P4	0.8	0.22	27.5
P5	2.2	0.22	10.0
P6	2.4	0.22	9.2

Table 3: Error estimates for the accumulated wind-driven rain measured at the south-west facade for the rain event of September 25th, 2007.

WDR gauge	S_{wdr} (mm)	E_{wdr} (mm)	e_{wdr} (%)
P2	2.0	0.08	4.0
P4	1.5	0.08	5.3
P5	2.9	0.08	2.8
P6	3.0	0.08	2.7